The Astrophysical Journal, 916:34 (15pp), 2021 July 20 https://doi.org/10.3847/1538-4357/abfe59

Building Robust Active Galactic Nuclei Mock Catalogs to Unveil Black Hole Evolution and for Survey Planning

V. Allevato[1,2,3], F. Shankar[4], C. Marsden[4], U. Rasulov[4], A. Viitanen[3,5], A. Georgakakis[6], A. Ferrara[1], and A. Finoguenov[3]

[1] Scuola Normale Superiore, Piazza dei Cavalieri 7, I-56126 Pisa, Italy
[2] INAF–Osservatorio di Astrofisica e Scienza delle Spazio di Bologna, OAS, Via Gobetti 93/3, 40129 Bologna, Italy
[3] Department of Physics, University of Helsinki, PO Box 64, FI-00014 Helsinki, Finland
[4] School of Physics and Astronomy, University of Southampton, Highfield, SO17 1BJ, UK
[5] Helsinki Institute of Physics, Gustaf Hällströmin katu 2, University of Helsinki, Finland
[6] Institute for Astronomy & Astrophysics, National Observatory of Athens, V. Paulou & I. Metaxa, 11532, Greece
Received 2021 February 19; revised 2021 April 28; accepted 2021 May 4; published 2021 July 22

Abstract

The statistical distributions of active galactic nuclei (AGNs), i.e., accreting supermassive black holes (BHs), in mass, space, and time are controlled by a series of key properties, namely, the BH–galaxy scaling relations, Eddington ratio distributions, and fraction of active BH (duty cycle). Shedding light on these properties yields strong constraints on the AGN triggering mechanisms while providing a clear baseline to create useful mock catalogs for the planning of large galaxy surveys. Here we delineate a robust methodology to create mock AGN catalogs built on top of large *N*-body dark matter simulations via state-of-the-art semiempirical models. We show that by using as independent tests the AGN clustering at fixed X-ray luminosity, galaxy stellar mass, and BH mass, along with the fraction of AGNs in groups and clusters, it is possible to significantly narrow down the choice in the relation between BH mass and host galaxy stellar mass, the duty cycle, and the average Eddington ratio distribution, delivering well-suited constraints to guide cosmological models for the coevolution of BHs and galaxies. Avoiding such a step-by-step methodology inevitably leads to strong degeneracies in the final mock catalogs, severely limiting their usefulness in understanding AGN evolution and in survey planning and testing.

Unified Astronomy Thesaurus concepts: Active galactic nuclei (16); Active galaxies (17); X-ray active galactic nuclei (2035); AGN host galaxies (2017); Large-scale structure of the universe (902)

1. Introduction

Several semianalytical models and hydrodynamical simulations (e.g., Springel et al. 2005; Hopkins et al. 2006; Menci et al. 2008) have been developed in recent years to describe the main mechanisms that fuel the central supermassive black holes (BHs). With a suitable adjustment of parameters, these models can explain many aspects of active galactic nucleus (AGN) phenomenology (e.g., Hopkins et al. 2006, 2008). Often relying on a rather heavy parameterization of the physics regulating the cooling, star formation, feedback, and merging of baryons (e.g., Monaco et al. 2007), semianalytical models of galaxy evolution can present serious degeneracies (e.g., González et al. 2011; Lapi et al. 2018) or even significant divergences in, e.g., the adopted subgrid physics (Scannapieco et al. 2012; Nuñez-Castiñeyra et al. 2020). Semiempirical models (SEMs) represent an original and complementary methodology to more traditional modeling approaches (e.g., Hopkins & Hernquist 2009). The aim of SEMs is to tackle specific aspects of galaxy and BH evolution in a transparent, fast, and flexible way, relying on just a few input assumptions and parameters. The SEMs cannot replace ab initio models of galaxy and BH evolution but can provide guidance to reduce the space of parameters and shed light on the viable physical processes.

Particularly relevant is the application of SEMs to the creation of active and normal galaxy mock catalogs (e.g., Conroy & White 2013), which are a vital component of the planning of imminent extragalactic surveys such as Euclid (Laureijs et al. 2011) and the Vera C. Rubin Observatory Legacy Survey of Space and Time (LSST; LSST Science Collaboration et al. 2009). The first step for the creation of mocks consists of assigning galaxies to dark matter halos extracted from large cosmological *N*-body simulations (e.g., Riebe et al. 2013; Klypin et al. 2016) via abundance-matching techniques (e.g., Kravtsov et al. 2004; Vale & Ostriker 2004; Shankar et al. 2006; Behroozi et al. 2013a; Moster et al. 2013). Despite being based on minimal assumptions, the latter are not immune to important systematics, mostly related to the input data, which propagate onto the star formation and mass assembly histories predicted by SEMs (e.g., Grylls et al. 2020b, 2020a; O'Leary et al. 2021).

In the last few years, several studies have focused on the creation of mock catalogs specifically for AGNs that can be utilized for the planning and testing of large-scale AGN-dedicated extragalactic surveys such eROSITA (e.g., Comparat et al. 2019; Georgakakis et al. 2019; Aird & Coil 2021). These AGN mocks are built by starting from an empirical galaxy catalog and assigning to each object a specific accretion rate that is proportional to the quantity L_X/M_{star}, drawn randomly from observationally determined probability distributions P_{AGN} (L_X/M_{star}; e.g., Bongiorno et al. 2016; Georgakakis et al. 2017; Aird et al. 2018). This quantity can be measured directly from observations and provides an estimate of X-ray emission per unit stellar mass for a galaxy. The advantage of this methodology is that by using just a few input relations, namely, the stellar mass–halo mass relation (from abundance matching) and the probability distribution of specific accretion rate P_{AGN}, it allows the creation of a mock catalog of AGNs that—by design—reproduces the observed X-ray luminosity function (XLF) and broadly matches the large-scale bias at a

given host galaxy stellar mass. Using this approach, Georgakakis et al. (2019) populated cosmological simulations with AGNs and showed that their clustering properties (including the signal at small scales) are consistent with state-of-the-art observational measurements of X-ray or UV/optically selected samples at different redshifts and accretion luminosities, supporting the view that the large-scale distribution of AGNs may be independent of the detailed physics of BH fueling. Some recent works also tested the same methodology against the large-scale bias dependence on the X-ray luminosity at different redshifts (Georgakakis et al. 2019; Aird & Coil 2021).

However, in these models, key information such as BH mass is largely bypassed, and the AGN duty cycle (i.e., the probability of a galaxy being active above a certain luminosity or threshold) is not considered as a separate model input parameter, limiting the efficacy of these models in shedding light on the processes controlling the coevolution of BHs and their hosts. Moreover, in these models, the assignment of specific accretion rates to mock galaxies by using $P_{\rm AGN}$ is a stochastic process, assumed to be independent of the environment (centrals and satellites of similar stellar mass share the same probability of being active).

In this paper, we instead create mock catalogs of AGNs by varying different input model parameters, namely the stellar mass–halo mass and BH mass–stellar mass relations, the AGN duty cycle, the Eddington ratio distribution, and the fraction of satellite AGNs (controlled by the parameter Q, defined later), and test the effect on several observables, such as the AGN XLF, the $P_{\rm AGN}$ distribution, and the AGN large-scale bias as a function of BH/stellar mass and luminosity. More generally, we demonstrate in this study that calibrating the AGN mocks on the bias at fixed BH mass, stellar mass, and AGN luminosity provides a self-consistent and robust route to break the most relevant degeneracies and narrow down the choice of input parameters. For example, Shankar et al. (2020) emphasized that current measurements of AGN clustering at $z = 0.25$ (Krumpe et al. 2015) are already sufficient to constrain, in ways independent of the AGN duty cycle, the scaling relations of BHs (e.g., Kormendy & Ho 2013; Reines & Volonteri 2015; Savorgnan & Graham 2016; Shankar et al. 2016; Davis et al. 2018). The main goal of this paper is to provide a complete framework to build a robust and realistic AGN mock catalog that is both consistent with many different and independent observables and physically sound, being based on the underlying scaling relations between BHs and their host galaxies and dark matter halos.

2. Research Methodology

In this section, we provide a step-by-step description of our baseline methodology.

1. At a given redshift of reference, in this work $z = 0.1$, we extract large catalogs of dark matter halos and subhalos from large, N-body dark matter simulations. We here rely on the MultiDark simulation (Riebe et al. 2013). The catalogs contain both central/parent halos and satellite halos with unstripped mass at infall.
2. To each parent halo, a central galaxy is assigned, with stellar mass given by abundance-matching relations at the redshift of reference (e.g., Grylls et al. 2019), while satellite halos are assigned a stellar mass at their redshift of infall.
3. To each galaxy, we assign a BH mass from an empirical BH mass–galaxy mass relation drawn from several recent studies (e.g., Shankar et al. 2016).
4. To each galaxy and BH, we then assign an Eddington ratio $\lambda = L_{\rm bol}/L_{\rm Edd}$, with $L_{\rm bol}$ the bolometric luminosity and $L_{\rm Edd}$ the Eddington limit of the BH. The parameter λ is randomly extracted from a $P(\lambda)$ distribution described by a Schechter function, the latter chosen in such a way as to reproduce the AGN XLF at $z = 0.1$, for a given input "duty cycle" (see below). In our reference model, we ignore, for simplicity, any mass dependence of $P(\lambda)$ on, e.g., BH mass. We will discuss in Section 5 the (moderate) impact of relaxing this assumption. Regardless, we note that any mass dependence in $P(\lambda)$ is degenerate with the duty cycle (e.g., in the AGN XLF; Shankar et al. 2013), a model input parameter we explore thoroughly in this work.
5. To each galaxy/BH, an extinction-corrected X-ray luminosity $L_{\rm X}$ in the 2–10 keV band is then assigned from the bolometric luminosity $L_{\rm bol}$ via up-to-date bolometric corrections (e.g., Duras et al. 2020).
6. Each galaxy and its associated BH is assigned a duty cycle, i.e., a probability for a BH of a given $M_{\rm BH}$ of being active, following empirically based duty cycles (e.g., Man et al. 2019).

We then generate our mock catalog of AGNs and, by varying our input parameters, test a number of outputs, such as the AGN XLF, the AGN specific accretion rate distribution $P_{\rm AGN}$, and the AGN large-scale clustering. We focus on $z = 0.1$, where the galaxy–BH scaling relations are better constrained and additional measurements on some of the key observables, such as AGN–galaxy clustering, are available. We stress that the methodology we put forward in this work is applicable to any redshift of interest. In Viitanen et al. 2021, for example, we apply our methodology to $z \sim 1.2$, while in Carraro et al. 2021, we push our methodology up to $z \sim 3$ and specifically focus on the correlation with star formation rate, which is not explicitly included in the present work.

2.1. Connecting Halos to Galaxies and BHs

We start from a large catalog of dark matter halos and subhalos from MultiDark[7]-Planck 2 (MDPL2; Riebe et al. 2013) at the redshift $z = 0.1$. The MDPL2 currently provides the largest publicly available set of high-resolution and large-volume N-body simulations (box size of 1000 h^{-1} Mpc, mass resolution of $1.51 \times 10^9\ h^{-1}\ M_{\odot}$). The ROCKSTAR halo finder (Behroozi et al. 2013b) has been applied to the MDPL2 simulations to identify halos and flag those (subhalos) that lie within the virial radius of a more massive host halo. The mass of the dark matter halo is defined as the virial mass in the case of host halos and the infall progenitor virial mass for subhalos.

From abundance-matching techniques, one can infer the stellar mass–halo mass relation, which shows that the baryons are converted into stars with very different efficiencies in halos of diverse mass (e.g., Shankar et al. 2006; Moster et al. 2013). We adopt the parameterization for the stellar-to-halo mass ratio

[7] www.cosmosim.org

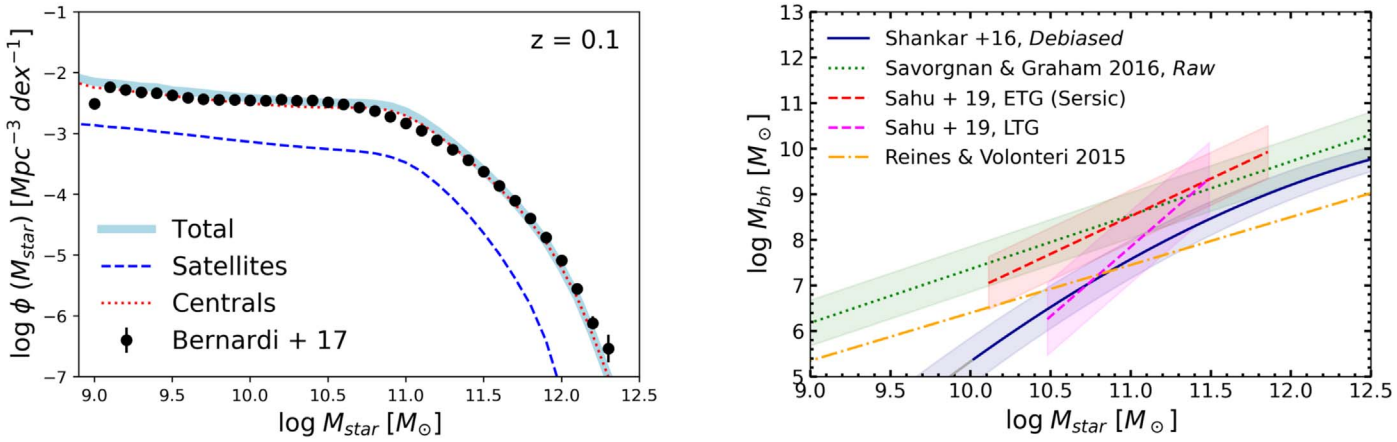

Figure 1. Left panel: stellar mass function at $z = 0.1$ for central and satellite mock galaxies, compared with measurements using SDSS DR7 galaxies. Right panel: BH mass–stellar mass relation, as put forward by Shankar et al. (2016, debiased) and derived for local galaxy samples with dynamically measured BH masses from Savorgnan & Graham (2016, raw). The $M_{\rm BH}$–$M_{\rm star}$ relations as derived for early- and late-type galaxies by Sahu et al. (2019) and AGNs by Reines & Volonteri (2015) are shown for comparison.

by Moster et al. (2013),

$$M_{\rm star}(M_h, z) = 2M_h N \left[\left(\frac{M_h}{M_n(z)} \right)^{-\beta(z)} + \left(\frac{M_h}{M_n(z)} \right)^{\gamma(z)} \right]^{-1}, \quad (1)$$

where N is the normalization of the stellar-to-halo mass ratio, M_n is a characteristic mass where the ratio is equal to the normalization N, and the two slopes β and γ indicate the behavior at the low and high halo mass ends, respectively. We fixed these redshift-dependent parameters as in Grylls et al. (2019), who suggested a steeper slope than Moster et al. (2013) for the high-mass end (as also shown in Shankar et al. 2014, 2017; Kravtsov et al. 2018), which better fits the Sloan Digital Sky Survey Data Release 7 (SDSS DR7) from Meert et al. (2015, 2016), with improved galaxy photometry.[8]

Figure 1 (left panel) shows the stellar mass functions at $z = 0.1$ presented in Bernardi et al. (2017), based on Sérsic-exponential fits to the surface brightness profiles of galaxies in the SDSS DR7 and characterized by significantly higher number densities of massive galaxies ($>10^{12}$ M_*) when compared to estimates by, e.g., Bell et al. (2003), Bernardi et al. (2010), Baldry et al. (2012), and Moustakas et al. (2013).

2.2. *Input* M_{BH}–M_{star} *Relation*

As a second step, to each galaxy, we assign a BH mass assuming the following two scaling relations.

1. The BH mass–stellar mass relation as derived in Shankar et al. (2016, hereafter BHSMR-Sha16 debiased),

$$\log \frac{M_{\rm BH}}{M_\odot} = 7.574 + 1.946 \log \left(\frac{M_{\rm star}}{10^{11} M_\odot} \right) - 0.306 \times \left[\log \left(\frac{M_{\rm star}}{10^{11} M_\odot} \right) \right]^2 - 0.011 \left[\log \left(\frac{M_{\rm star}}{10^{11} M_\odot} \right) \right]^3, \quad (2)$$

with a mass-dependent intrinsic scatter given by

$$\Delta \log \frac{M_{\rm BH}}{M_\odot} = 0.32 - 0.1 \times \log \left(\frac{M_{\rm BH}}{M_\odot} \right), \quad (3)$$

as presented in Equation (5) of Shankar et al. (2019). Note that this equation is applicable to galaxies with stellar masses $\log M_{\rm star}/M_\odot \gtrsim 10$.

2. The relation derived for the Savorgnan & Graham (2016) sample of galaxies with dynamically measured BH masses, hereafter BHSMR-SG16 (raw), as presented in Equation (3) of Shankar et al. (2019), with a scatter of 0.5 dex:

$$\log \frac{M_{\rm BH}}{M_\odot} = 8.54 + 1.18 \log \left(\frac{M_{\rm star}}{10^{11} M_\odot} \right). \quad (4)$$

The right panel of Figure 1 shows the $M_{\rm BH}$–$M_{\rm star}$ relations defined by Equations (2) and (4) with their associated dispersions and compared with several other relations from the recent literature, as labeled. It can be seen from Figure 1 that our two chosen relations bracket the systematic uncertainties in both slope and normalization present in the local BH mass–galaxy stellar mass relation.

In our reference models throughout, we include the scatters in the relations described above as random normal dispersions. However, it may be possible that some correlation between, in particular, the dispersions in BH mass and galaxy stellar mass at a given DM halo mass may exist. We thus explore in Section 5 some of the main consequences for our results of including a degree of covariance in the scatters and refer to Viitanen et al. (2021) for a more comprehensive discussion of implementing a covariant scatter in the input stellar mass–halo mass and BH mass–stellar mass relations.

2.3. *Input Eddington Ratio Distribution*

To each galaxy and BH, we assign an Eddington ratio $\lambda \equiv L_{\rm bol}/L_{\rm Edd}$ following a $P(\lambda)$ distribution described by the following.

[8] We decrease by 0.1 dex the original stellar masses by Grylls et al. (2019) to further improve the match to the latest stellar mass function by Bernardi et al. (2017).

1. A Schechter function,

$$P(\lambda) \propto \left(\frac{\lambda}{\lambda^{\star}}\right)^{-\alpha} \exp\left(-\frac{\lambda}{\lambda^{\star}}\right), \quad (5)$$

with λ in the range $\lambda = 10^{-4}$–10^{1}. The Schechter function is characterized by two free parameters: the knee $\lambda^{\star}$, where the power-law form of the function cuts off, and the power-law index α. The Schechter function is supported by recent studies of the specific accretion rate distribution of AGNs, such as Bongiorno et al. (2016), Aird et al. (2017, 2018, 2019), and Georgakakis et al. (2017).

2. A Gaussian function,

$$P(\log(\lambda)) \propto \exp\left(-\frac{[\log(\lambda) - \mu]^2}{2\sigma^2}\right), \quad (6)$$

where $\log(\lambda)$ varies in the range $\log \lambda = -4$–1, σ is the standard deviation, and μ is the mean of the distribution.

Both the Schechter and Gaussian input $P(\lambda)$ are normalized to unity. Such Eddington ratio distributions have a lower cutoff at $\lambda_{\rm min} = 10^{-4}$, below which the sources are no longer regarded as AGNs. We choose $\lambda_{\rm min}$ to be low enough to include even the faintest AGN recorded in the $z = 0.1$ AGN XLF, down to $\log L_{\rm X} \sim 41$ erg s^{-1} for BHs with mass $\log M_{\rm BH} \gtrsim 6$. We note that the exact choice of $\lambda_{\rm min}$ is not too relevant in our modeling. Lowering/increasing $\lambda_{\rm min}$ would simply correspond to a higher/lower duty cycle, i.e., a higher/lower probability for BHs to active. In Section 5, we explore the effect on our results of assuming an input BH mass–dependent Eddington ratio distribution, i.e., $P(\lambda, M_{\rm BH})$.

We then assign a bolometric luminosity to each source according to the Eddington ratio λ and the BH mass. The bolometric luminosity is then converted into intrinsic rest-frame 2–10 keV X-ray luminosity via the relation $L_{\rm X} = L_{\rm bol}/K_{\rm X}$, with the bolometric correction $K_{\rm X}$ expressed as

$$K_{\rm X}(L_{\rm bol}) = a\left[1 + \left(\frac{\log(L_{\rm bol}/L_{\odot})}{b}\right)^{c}\right] \quad (7)$$

with $a = 10.96$, $b = 11.93$, and $c = 17.79$ (Duras et al. 2020).

2.4. Input BH Duty Cycle

In general terms, the total accretion probability of a BH being active at a given Eddington ratio is a convolution of the duty cycle $U(M_{\rm BH})$, i.e., the probability of a galaxy/BH being active as an AGN above a certain luminosity threshold and the (normalized) Eddington ratio distribution $P(\lambda)$ being accreting at a given rate (e.g., Steed & Weinberg 2003; Marconi et al. 2004; Aversa et al. 2015). We here follow the rather common and broad approximation followed in the continuity equation formalism of expressing the total accretion probability into a simple product of the duty $U(M_{\rm BH})$ and the Eddington ratio distribution $P(\lambda)$ (e.g., Small & Blandford 1992; Marconi et al. 2004; Shankar et al. 2009). This choice is extremely flexible and allows us to disentangle the roles of a mass- and/or time-dependent duty cycle from an evolving characteristic Eddington ratio λ (e.g., Shankar et al. 2013).

Both the Eddington ratio distribution $P(\lambda)$ and duty cycle $U(M_{\rm BH})$ have been separately studied by different groups. For the duty cycle in particular, despite the numerous dedicated works, no clear trend has yet emerged, and controversial results

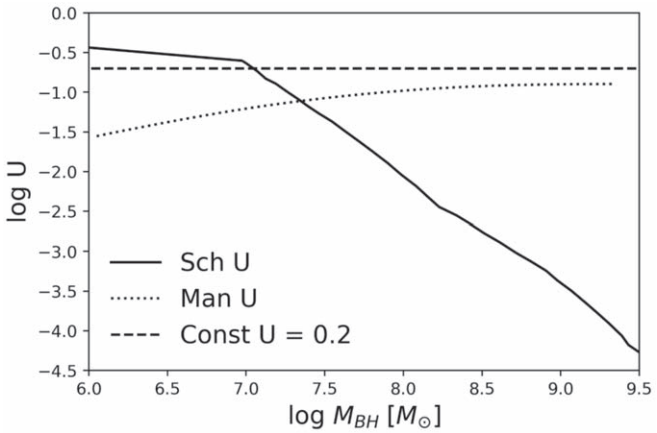

Figure 2. Duty cycle U as a function of $M_{\rm BH}$ as derived in Schulze & Wisotzki (2010, solid line) at $z = 0.1$, Man et al. (2019, dotted line) at $z < 0.1$, and Goulding et al. (2010, dashed line).

are present in the literature. For this reason, we decided to test three different duty cycles for BHs with mass $\log(M_{\rm BH}/M_{\odot}) \gtrsim 6$, as shown in Figure 2:

1. a duty cycle $U(M_{\rm BH})$ decreasing with BH mass, as derived in Schulze & Wisotzki (2010) at $z = 0.1$ for Compton-thin un/obscured AGNs, hereafter U-SW10 (decr);
2. a duty cycle increasing with BH mass in such a way as to reproduce the increasing trend with host galaxy stellar mass as estimated at low redshift ($z < 0.1$) by Man et al. (2019) for narrow-line AGNs in host galaxies with $\log(M_{\rm star}/[M_{\odot}]) > 9$, hereafter U-M19 (incr); and
3. a constant duty cycle $U(M_{\rm BH}$ or $M_{\rm star}) = 0.2$, as suggested by Goulding et al. (2010), hereafter U-G10 (const).

In all cases, we define a duty cycle as the probability of BHs being active above the minimal Eddington ratio threshold $\lambda_{\rm min}$ in our input $P(\lambda)$ distribution. It is worth noticing that we are assuming that the duty cycle from Man et al. (2019) can be applied to both obscured and unobscured AGNs. Given that it has been derived by using a sample of narrow-line AGNs, we can consider it as a lower limit. However, a similar duty cycle increasing with stellar mass was also derived in Georgakakis et al. (2017) from a sample of Compton-thin un/obscured AGNs.

2.5. The Q Parameter

The AGN duty cycle $U(M_{\rm BH})$ is the average fraction of both central and satellite galaxies that are active at a given stellar or BH mass above a given threshold. However, the relative probability of a central and satellite BH being active could still be different. To allow for this possibility, following Shankar et al. (2020), we define the total duty cycle as the sum of the fraction of active central and satellite BHs at a given BH mass, i.e., $U(M_{\rm BH}) = U_c(M_{\rm BH}) + U_s(M_{\rm BH})$, with U_c and U_s the duty cycles of, respectively, central and satellite galaxies above a given luminosity or Eddington ratio threshold. We can then define the parameter $Q = U_s/U_c$ as the relative probability of satellite and central AGNs being active. Constraining the Q parameter would be, of course, of key importance to shed light on the different AGN triggering mechanisms. For example, a high value of Q would point toward satellites being preferentially active rather than centrals of similar mass, a

Table 1
Model Input Parameters

$M_{\rm star}$–$M_{\rm BH}$	U	$P(\lambda)$	$\log\lambda^{\star}$ (or $\log\mu$)	α (or σ)	$\log\langle\lambda_{\rm AR}\rangle$
Sha16 (debiased)	Schulze & Wisotzki (2010)	Schechter	−0.45	0.15	31.81
Sha16 (debiased)	Man et al. (2019)	Schechter	−1.8	−0.15	31.56
Sha16 (debiased)	Goulding et al. (2010)	Schechter	−1.9	0	31.56
SG16 (raw)	Schulze & Wisotzki (2010)	Schechter	−1.3	−0.35	32.93
SG16 (raw)	Man et al. (2019)	Schechter	−2.5	0.4	31.8
SG16 (raw)	Goulding et al. (2010)	Schechter	−2.4	0.8	31.42
Sha16 (debiased)	Schulze & Wisotzki (2010)	Gaussian	−2.8	1	31.69
Sha16 (debiased)	Man et al. (2019)	Gaussian	−4	1	31.51
Sha16 (debiased)	Goulding et al. (2010)	Gaussian	−4	1.1	31.24
SG16 (raw)	Schulze & Wisotzki (2010)	Gaussian	−3	1.1	32.62
SG16 (raw)	Man et al. (2019)	Gaussian	−4.5	1.3	31.71
SG16 (raw)	Goulding et al. (2010)	Gaussian	−4.5	1.4	31.41

condition that would be difficult to reconcile with a strict merger-only scenario but possibly still consistent with disk instability processes (e.g., Gatti et al. 2016).

Previous studies in the literature always assumed $Q = 1$ (noticeable exceptions are Allevato et al. 2019; Shankar et al. 2020), implying that all central and satellite galaxies share equal probabilities of being active (e.g., Comparat et al. 2019; Aird & Coil 2021). The Q parameter can, in principle, be directly measured from the fraction of satellite galaxies in groups and clusters of galaxies $f_{\rm sat}^{\rm AGN}$ (see Gatti et al. 2016, and references therein). In fact, the Q parameter can be expressed in terms of $f_{\rm sat}^{\rm AGN}$ as $Q = f_{\rm sat}^{\rm AGN}(1 - f_{\rm sat}^{\rm BH})/[1 - f_{\rm sat}^{\rm AGN}]f_{\rm sat}^{\rm BH}$, where $f_{\rm sat}^{\rm BH} = N_s/(N_s + N_c)$ is the total fraction of (active and nonactive) BHs in satellites with host galaxy stellar masses within $M_{\rm star}$ and $M_{\rm star} + dM_{\rm star}$ (for full details, see Shankar et al. 2020).

3. Outputs

We then consider different outputs of our mock catalog of galaxies and BHs at a given z.

1. The AGN XLF,

$$\Phi_{\rm AGN}(L_{\rm X}) = \int_{\log\lambda_{\rm min}} P(\lambda \propto L_{\rm X}/M_{\rm BH}) \times U(M_{\rm BH})\,\Psi(M_{\rm BH})\,{\rm dlog}\lambda, \quad (8)$$

where $\Psi(M_{\rm BH}) = \Psi_{\rm AGN}(M_{\rm BH})/U(M_{\rm BH})$ is the total (active and nonactive) BH mass function, $U(M_{\rm BH})$ is the AGN duty cycle, and $P(\lambda)$ is the normalized Eddington ratio distribution with $\log\lambda_{\rm min} = -4$.

1. The specific accretion rate distribution,

$$P_{\rm AGN}(\lambda \propto L_{\rm X}/M_{\rm star}) = \int_{\log\lambda_{\rm min}} P(\lambda \propto L_{\rm X}/M_{\rm star}) \times U(M_{\rm star})\,{\rm dlog}\lambda, \quad (9)$$

where $\lambda \propto L_{\rm X}/M_{\rm star}$ defines the rate of accretion onto the central BH scaled relative to the stellar mass of the host galaxy, and $P_{\rm AGN}$ describes the probability of a galaxy hosting an AGN of a given $L_{\rm X}/M_{\rm star}$ at a given redshift. We can also define the characteristic $\langle\lambda\rangle$ of the specific accretion rate distribution as

$$\langle\lambda\rangle = \frac{\int\lambda\,P_{\rm AGN}(\lambda)\,{\rm dlog}\lambda}{\int P_{\rm AGN}(\lambda)\,{\rm dlog}\lambda}. \quad (10)$$

At variance with many other previous approaches, our flexible methodology based on an input duty cycle and Eddington ratio distribution allows us to use the $P_{\rm AGN}$ distribution as an output rather than an input of our AGN mock catalog, thus providing an additional valuable constraint independent of AGN clustering. We will show that the $P_{\rm AGN}$ distribution is particularly useful in constraining the viable duty cycles and the underlying BH–galaxy scaling relations.

1. The large-scale bias of mock AGNs with BH mass (and, similarly, stellar mass) in the range $\log M_{\rm BH}$ and $\log M_{\rm BH} + d\log M_{\rm BH}$ following the formalism of Shankar et al. (2020),

$$b = \left[\sum_{i=1}^{N_c} U_{c,i}(M_{\rm BH})\,b_{c,i}(M_{\rm BH}) + \sum_{i=1}^{N_s} U_{s,i}(M_{\rm BH})\,b_{sat,i}(M_{\rm BH})\right] \Bigg/ \left[\sum_{i=1}^{N_{cen}} U_{c,i}(M_{\rm BH}) + \sum_{i=1}^{N_s} U_{s,i}(M_{\rm BH})\right] \quad (11)$$

where $U_c(M_{\rm BH}) = U(M_{\rm BH})N(M_{\rm BH})/(N_c(M_{\rm BH}) + QN_s(M_{\rm BH}))$ is the duty cycle of the central $U_s(M_{\rm BH}) = QU_c(M_{\rm BH})$ is the duty cycle of the satellite AGN, and $N(M_{\rm BH}) = N_c(M_{\rm BH}) + N_s(M_{\rm BH})$ is the number of central and satellite galaxies in the stellar mass bin $M_{\rm BH}$ and $M_{\rm BH} + dM_{\rm BH}$. Similarly, the AGN large-scale bias can be estimated as a function of BH mass.

4. Results

4.1. AGN XLF and P_{AGN}

We now use the model described in the previous section to create mock catalogs of AGNs. We vary the input parameters and study how these changes affect the outputs, such as the AGN XLF and the specific accretion rate distribution $P_{\rm AGN}$. We consider various different cases, and each combination of model input parameters is shown in Table 1.

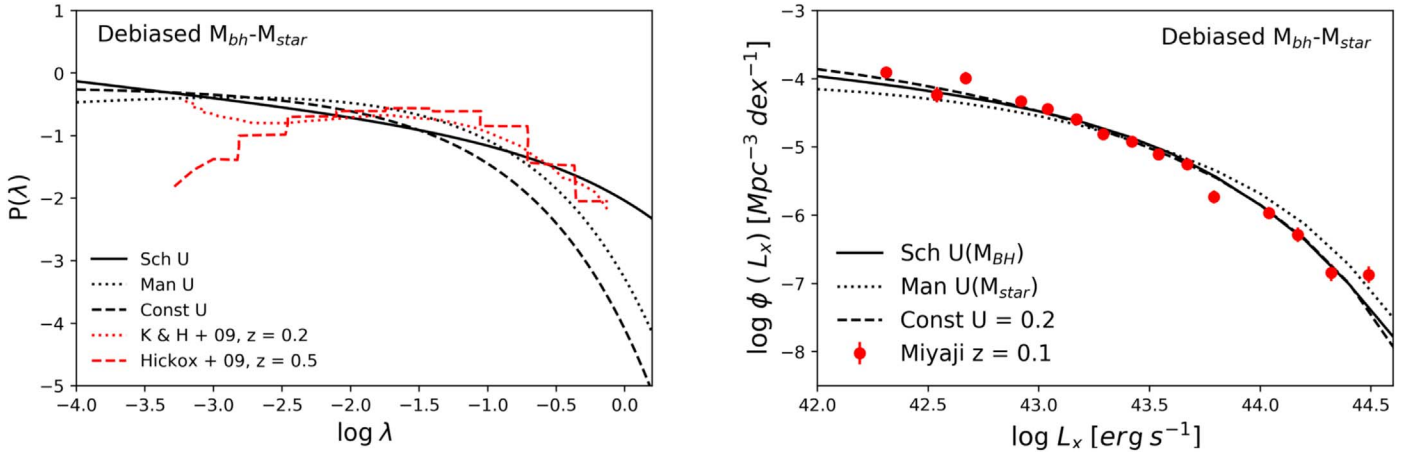

Figure 3. Left panel: input Eddington ratio distribution $P(\lambda)$, described by a Schechter function characterized by a knee $\lambda^{\star}$ and a power-law index α derived to reproduce the AGN luminosity, when using the BH mass–stellar mass relation from Shankar et al. (2006, debiased) and the AGN duty cycle derived by Schulze & Wisotzki (2010, solid line), Man et al. (2019, dotted line), and Goulding et al. (2010, dashed line), compared to the results of Kauffmann & Heckman (2009, dotted red line) and Hickox et al. (2009, dashed red line). Right panel: corresponding XLF for mock AGNs at $z = 0.1$ compared to the XLF as derived for Compton-thin un/obscured AGNs in Miyaji et al. (2015).

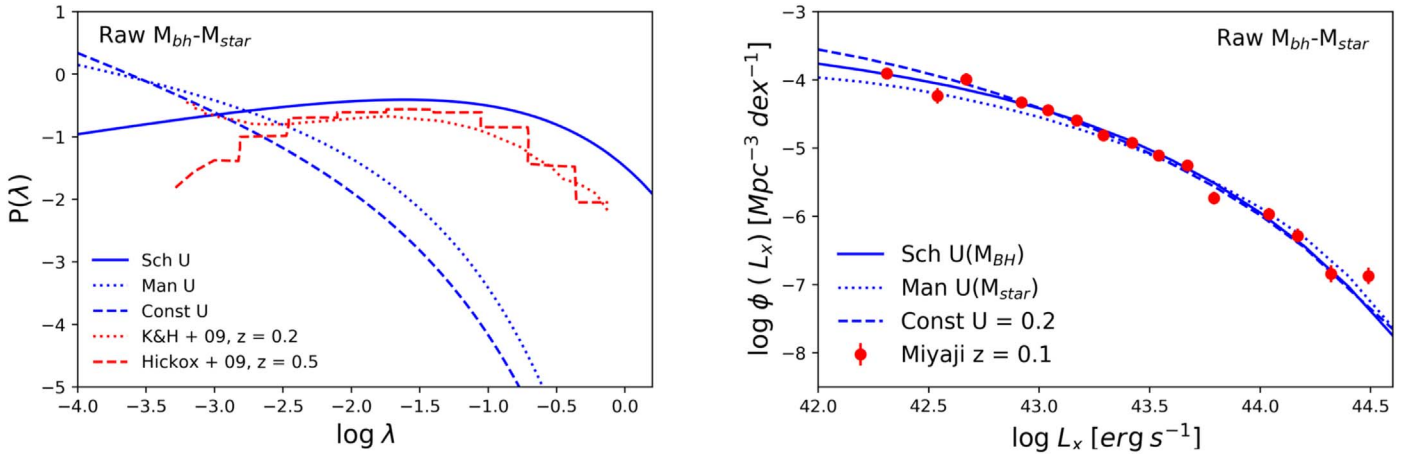

Figure 4. Left panel: input Eddington ratio distribution $P(\lambda)$, described by a Schechter function characterized by a knee $\lambda^{\star}$ and a power-law index α derived to reproduce the AGN luminosity function, when using the BH mass–stellar mass relation from Savorgnan & Graham (2016, raw) and the AGN duty cycle derived by Schulze & Wisotzki (2010, solid line) and Man et al. (2019, dotted line) and assuming a constant $U = 0.20$ (Goulding et al. 2010, dashed line), compared to the results of Kauffmann & Heckman (2009, dotted red line) and Hickox et al. (2009, dashed red line). Right panel: corresponding XLF for mock AGNs at $z = 0.1$ compared to the XLF as derived for Compton-thin un/obscured AGNs in Miyaji et al. (2015).

We estimate the XLF $\Phi_{\rm AGN}$ (defined in Equation (8)) for the different duty cycles, setting the free parameters of the input $P(\lambda)$ distribution in order to reproduce the observationally inferred XLF of X-ray-selected AGNs at $z = 0.1$ (Miyaji et al. 2015). We infer the parameters of $P(\lambda)$ based on an overall match to an observational constraint, i.e. the AGN XLF, but we do not attempt formal χ^2 minimization because the errors themselves are not well defined enough to do so. We note where models fit observations within a plausible range of systematic uncertainties and where they do not. Our objective is to show how the different "observables" depend on the input model parameters and delineate a guideline for the creation of realistic AGN mock catalogs, so we are not inherently interested in the free parameters of $P(\lambda)$ that might better fit the (real) observations.

As a first case, we consider a $P(\lambda)$ described by a Schechter function. As shown in Figures 3 and 4, we can reproduce the observed AGN XLF as derived in Miyaji et al. (2015) for AGNs at $z = 0.1$ (or, similarly, in Ueda et al. 2014) independently of the choice of the input AGN duty cycle and BH mass–stellar mass relation. In particular, if we assume BHSMR–Sha16 (debiased), the input $P(\lambda)$ is characterized by a power-law index $\alpha \sim 0$, i.e., an almost constant probability as a function of Eddington ratio at $\lambda < \lambda^{\star}$. Assuming the AGN duty cycle U-SW10 (decr), the input $P(\lambda)$ is almost consistent with observations (i.e., Heckman & Kauffmann 2006; Hickox et al. 2009) with a knee $\log\lambda^{\star} = -0.45$. It is worth noting that these observations are calibrated on the $M_{\rm BH}$–σ relation of Tremaine et al. (2002) that would shift the Eddington ratio distribution to higher λ by a factor of $\sim$2, still in agreement with our AGN mock predictions. A smaller knee ($\log\lambda^{\star} \sim -2$) is obtained for mock AGNs assuming U-M19 (incr) and U-G10 (const). Similarly, we can reproduce the observed AGN XLF for different AGN duty cycles when assuming SG16 (raw) (see Figure 4). However, the corresponding input $P(\lambda)$ distributions of mock AGNs with U-M19 (incr) and U-G10 (const) are in tension with the data at similar redshifts (i.e., Hickox et al. 2009; Kauffmann & Heckman 2009).

We also derived the corresponding specific accretion rate distributions $P_{\rm AGN}$ defined in Equation (9) as the convolution

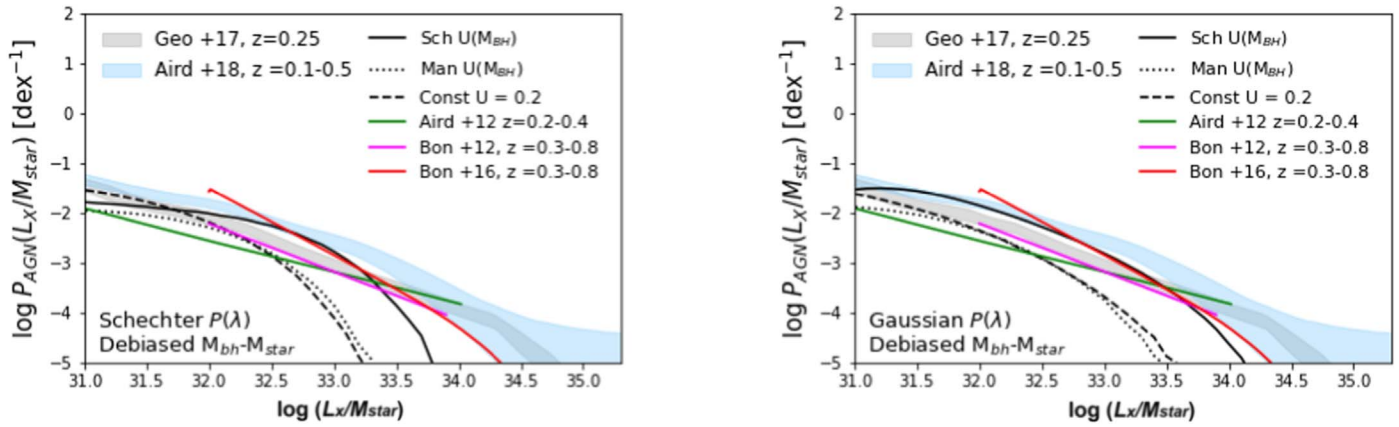

Figure 5. Specific accretion rate distribution $P_{\rm AGN}(\lambda \propto L_{\rm X}/M_{\rm star})$ defined as the probability that a galaxy of a given λ is an AGN and given by the convolution of the input Eddington ratio distribution $P(\lambda)$ and the AGN duty cycle (Equation (11)). The prediction from mock AGNs assuming a Schechter (left panel) and Gaussian (right panel) input $P(\lambda)$ and an $M_{\rm BH}$–$M_{\rm star}$ relation as defined in Shankar et al. (2006, debiased) are compared with data from Aird et al. (2012, 2018), Bongiorno et al. (2012, 2016), and Georgakakis et al. (2017), according to the legend.

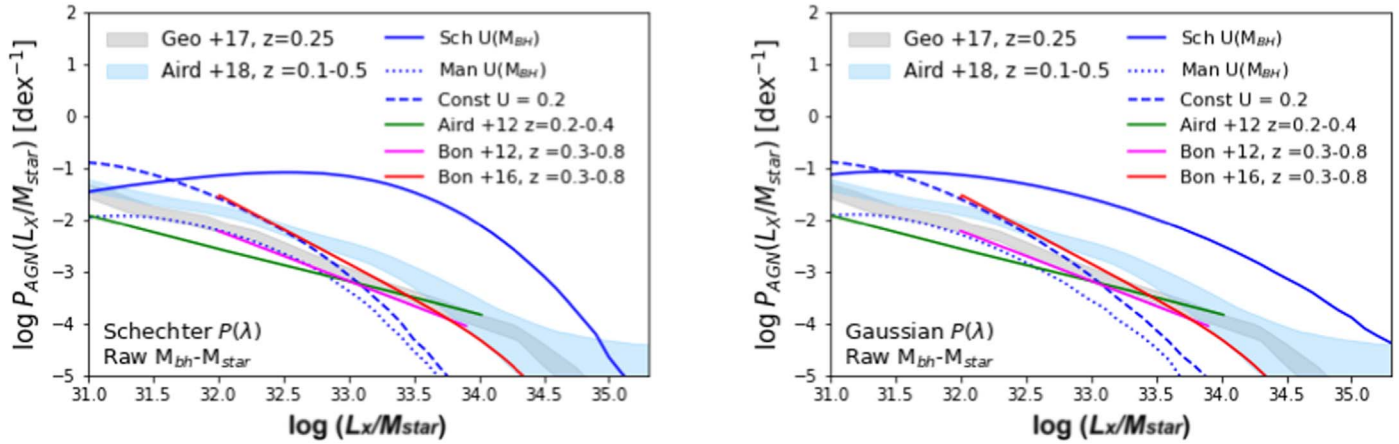

Figure 6. Specific accretion rate distribution $P_{\rm AGN}(\lambda \propto L_{\rm X}/M_{\rm star})$ defined as the probability that a galaxy of a given λ is an AGN and given by the convolution of the input Eddington ratio distribution $P(\lambda)$ and the AGN duty cycle (Equation (11)). The prediction from mock AGNs with a Schechter (left panel) and Gaussian (right panel) input $P(\lambda)$ and an $M_{\rm BH}$–$M_{\rm star}$ relation as defined in Savorgnan & Graham (2016, raw) are compared with data from Aird et al. (2012, 2018), Bongiorno et al. (2012, 2016), and Georgakakis et al. (2017), according to the legend.

of an input normalized $P(\lambda)$ and the AGN duty cycle U. We also applied a luminosity cut at $\log(L_{\rm X}/[{\rm erg\ s^{-1}}]) > 41$ to the mock AGNs in order to compare with recent observations based on X-ray-selected AGNs. As shown in Figures 5 and 6, $P_{\rm AGN}$ is affected by the input $P(\lambda)$ and duty cycles (for a given BH mass–stellar mass relation) and by the $M_{\rm star}$–$M_{\rm BH}$ relation (for a given duty cycle). It is immediately noteworthy that the specific accretion rate distribution mimics the shape of the input $P(\lambda)$, while the AGN duty cycle affects the characteristic $\langle\lambda\rangle$. In detail, assuming BHSMR–Sha16 (debiased) and setting U-SW10 (decr), the $P_{\rm AGN}$ distribution is more consistent with observations at similar redshifts (e.g., Aird et al. 2017; Georgakakis et al. 2017) and has a larger characteristic $\log\langle\lambda\rangle$ (=31.8 and 31.7 for a Schechter and Gaussian $P(\lambda)$, respectively) than using different U (see Table 1). However, the observationally derived specific accretion rate distributions are characterized by tails at high $L_{\rm X}/M_{\rm star}$ that are not present in our mock AGN predictions (see Section 5 for more discussion).

When we use BHSMR-SG16 (raw), the $P_{\rm AGN}$ distribution of mock AGNs is almost 1 order of magnitude higher at all $L_{\rm X}/M_{\rm star}$ than the data when using U-SW10 (decr). The $P_{\rm AGN}$ distribution of mock AGNs is more in line with observations when using U-M19 (incr) and U-G10 (const), at least at $\log L_{\rm X}/M_{\rm star} \leqslant 33$. However, the corresponding input Eddington ratio distributions $P(\lambda)$ are highly inconsistent with observations (see Figure 4).

It is worth noting that all of these results are derived for an $M_{\rm star}$–M_h relation given by Grylls et al. (2019) and independent of the particular choice of the Q parameter.

4.2. AGN Large-scale Bias

Each mock AGN resides in satellite or central halos with a given parent halo mass that corresponds to a specific value of the large-scale bias via the numerically derived correlation between halo mass and bias that we take from van den Bosch (2002) and Tinker et al. (2005), in line with what is assumed in the observational samples. We then derive the bias of the mock AGNs as a function of the host galaxy stellar mass and BH mass by using Equation (11) with different choices of the underlying duty cycles U, input stellar mass–halo mass, BH mass–stellar mass relations, and values of the Q parameter. In all of the model renditions considered below, the $P(\lambda)$ parameters are fixed in order to reproduce the AGN XLF.

Figure 7 shows the AGN large-scale bias as a function of BH mass and host galaxy stellar mass when using different (a) duty

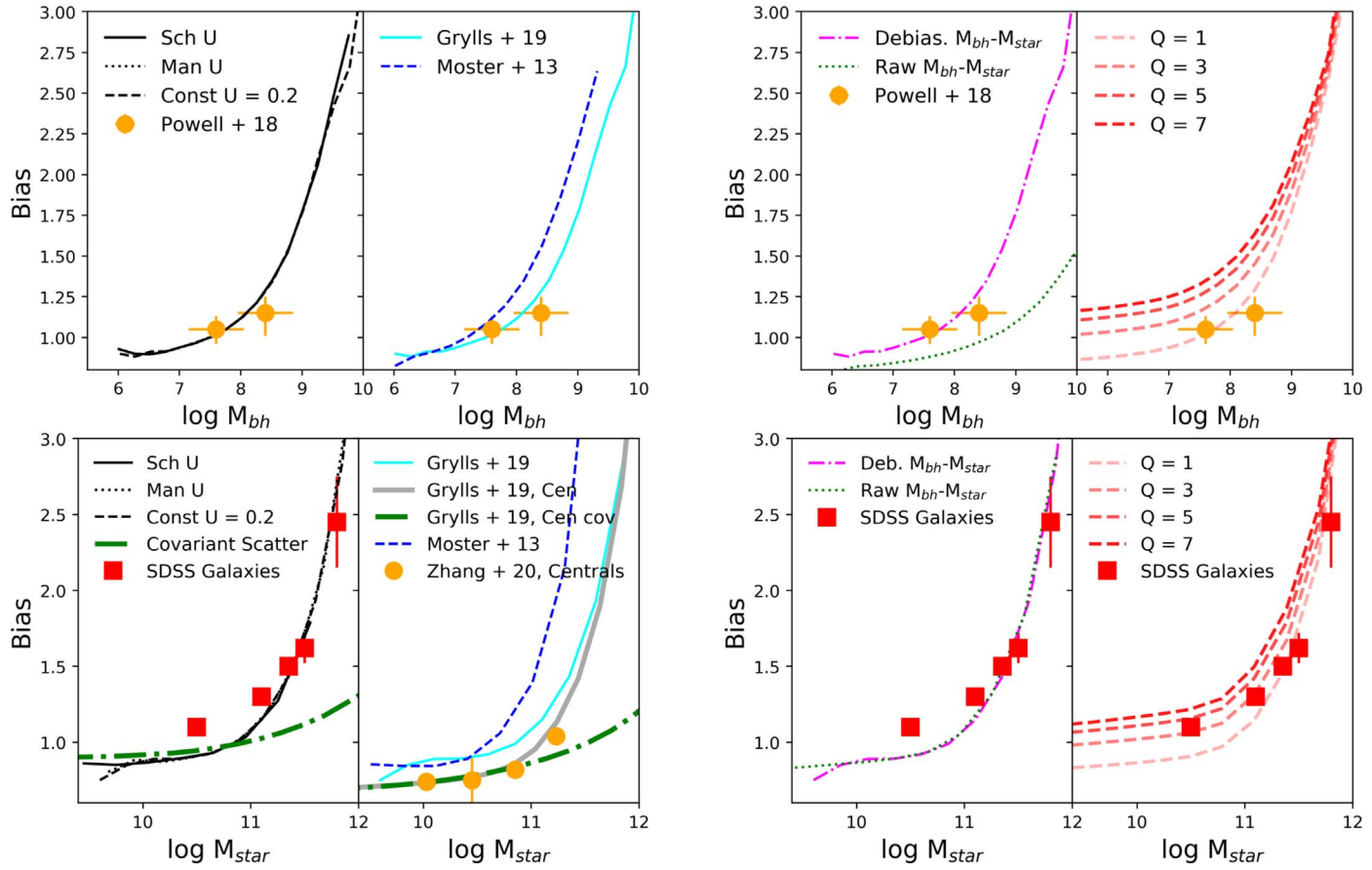

Figure 7. Large-scale bias of mock AGNs as a function of BH mass (upper panels) and host galaxy stellar mass (lower panels) when using different duty cycles, input stellar mass–halo mass and BH mass–stellar mass relations, and Q (see text for more details). The bias estimates as a function of $M_{\rm BH}$ from Powell et al. (2018) for X-ray-selected AGNs at $z \sim 0.04$, as a function of $M_{\rm star}$ from SDSS AGNs (Zhang et al. 2021, orange circles) and SDSS galaxies (Domínguez Sánchez et al. 2018, red squares; see the text for more details) in the local universe, are shown for comparison. The green dashed–dotted line shows the predictions when assuming a covariant scatter in the $M_{\rm star}$–M_h and $M_{\rm BH}$–$M_{\rm star}$ relations, as discussed in Section 5.

cycles (for fixed $M_{\rm star}$–M_h and $M_{\rm BH}$–$M_{\rm star}$ relations and Q), (b) input stellar mass–halo mass relations (for a fixed $M_{\rm BH}$–$M_{\rm star}$ relation, duty cycle, and Q), (c) input BH mass–stellar mass relations (for a fixed duty cycle, $M_{\rm star}$–M_h relation, and Q), and (d) Q values (for a fixed duty cycle and $M_{\rm star}$–M_h and $M_{\rm BH}$–$M_{\rm star}$ relations).

As expected, the large-scale bias as a function of BH mass mainly depends on the input BH mass–stellar mass relation and Q parameter, with a mild dependence on the $M_{\rm star}$–M_h relation (top panels of Figure 7). Conversely, the bias as a function of the AGN host galaxy stellar mass is only affected by Q, with a weak dependence on the input stellar mass–halo mass relation (bottom panels of Figure 7). In particular, mock AGNs with a given BH mass reside in more massive parent halos when assuming BHSMR–Sha16 (debiased) and/or $Q \gtrsim 2$. In the former case, the effect is stronger at large BH masses, while in the latter, it is mainly affecting small BH masses. These results are independent of the shape of the input $P(\lambda)$ distribution, either Gaussian or Schechter.

The comparison of our model predictions with large-scale bias estimates of X-ray-selected AGNs as a function of $M_{\rm BH}$ in the local universe (Powell et al. 2018) shows a degeneracy among the input model parameters. In fact, the observations can be reproduced by either BHSMR–Sha16 (debiased) with $Q = 1$ (using Grylls et al. 2019) or BHSMR-SG16 (raw) with $Q > 2$ and/or a stellar mass–halo mass relation given by Moster et al. (2013). It is worth noting that the BH masses in Powell et al. (2018) are derived by parameters calibrated on relations close to BHSMR-SG16 (raw). A better comparison with a model that assumes BHSMR–Sha16 (debiased) would imply a correction that moves the data to lower BH masses, strengthening the agreement among the observations and our model predictions.

Unfortunately, only few measurements are available at $z \leqslant 0.1$ of the AGN large-scale bias in bins of host galaxy stellar mass. In particular, recent estimates of the hosting central halo mass of SDSS AGNs (Zhang et al. 2021) suggest an $M_{\rm star}$–M_h relation in agreement with Grylls et al. (2019). To provide additional clustering constraints, we derived the two-point projected correlation function $w_p(r_p)$ in the range $r_p = 0.1$–$30\,h^{-1}$ Mpc as a function of stellar mass for the SDSS galaxies at $z < 0.1$ (Domínguez Sánchez et al. 2018). This sample has the same photometry and mass-to-light ratios as those adopted in the Bernardi et al. (2017) stellar mass function, which we adopt as a reference for our stellar mass–halo mass relation (Figure 1). We then converted $w_p(r_p)$ to bias estimates by making use of the projected two-point correlation function of the matter (Eisenstein & Hu 1999) with the same cosmology as in our reference dark matter simulation. The results are shown as red squares in the bottom left panel of Figure 7. The errors on the SDSS galaxy clustering measurements correspond to the square root of the covariance matrix

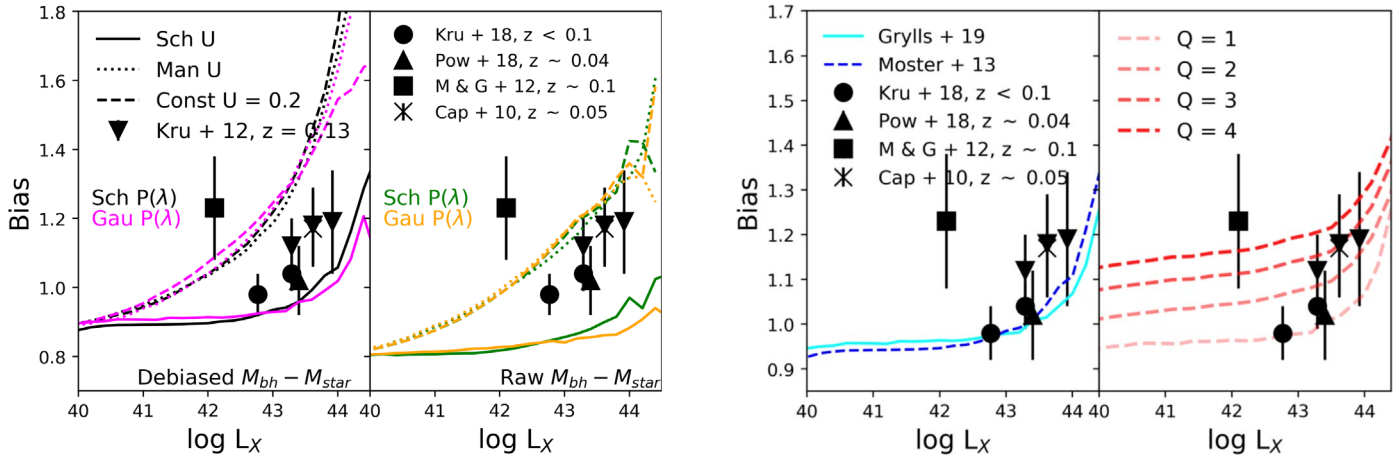

Figure 8. Large-scale bias vs. X-ray (2–10 keV) luminosity (in units of erg s^{-1}) for mock AGNs when using a decreasing (Schulze & Wisotzki 2010), increasing (Man et al. 2019), and constant ($U = 0.2$; Goulding et al. 2010) duty cycle as a function of BH mass, compared with bias estimates from previous studies at similar redshifts. For samples for which the AGN X-ray luminosity is estimated in an energy interval other than the 2–10 keV band, L_X(2–10 keV) is derived assuming a power-law X-ray spectrum with a photon index of $\Gamma = 1.9$.

diagonal elements calculated via the bootstrap resampling method.

Our predicted bias as a function of stellar mass nicely lines up with the SDSS galaxy bias measurements, especially for galaxies with mass $\log M_\star/M_\odot \gtrsim 11$, and, as expected, in ways fully independent of the duty cycle and the input BH mass–stellar mass relation. Our results thus strongly suggest that AGN mocks where the AGN activity is independent of environment (i.e., $Q \sim 1$) will guarantee a match to the galaxy clustering if the host galaxies are already turned against clustering measurements (we discuss possible caveats to this statement in Section 5).

Figure 6 shows that, despite the bias as a function of BH mass and galaxy stellar mass being an excellent observable to constrain the BH mass–stellar mass relation and the Q parameter, it is insensitive to AGN duty cycle. We discuss below how the AGN bias as a function of AGN luminosity can help to break the degeneracies in this fundamental input parameter.

As shown in Figure 8, the AGN bias as a function of Lx depends mostly on the AGN duty cycle and Q parameter (first and fourth panels), moderately on the BH mass–stellar mass relation (first and second panels), and weakly on the stellar mass–halo mass relation (third panel). The trends reported in the left panels of Figure 8 can be readily understood from the fact that an increasing duty cycle with BH mass (such as U-M19; dotted lines) necessarily implies, on average, lower Eddington ratios to reproduce the same luminosity function, as proportionally more massive BHs will be active in this model. In turn, lower Eddington ratios will map the same AGN luminosities to more massive BHs residing, on average, in more massive and clustered galaxies and dark matter halos. At a fixed duty cycle and Eddington ratio distribution, a lower normalization in the BH mass–stellar mass relation, such as in our BHSMR–Sha16 (debiased) case, would map the same luminosities to more massive/clustered galaxies.

At face value, the comparison with the large-scale AGN bias as a function of L_X estimated for X-ray-selected AGNs at $z \leqslant 0.1$ (e.g., Krumpe et al. 2018; Powell et al. 2018) favors models adopting the BHSMR–Sha16 (debiased) relation and decreasing duty cycles, as in our U-SW10 (decr) model (left panels), in ways largely independent of the shape of the input $P(\lambda)$ distribution. We note that the data could also be reproduced by assuming BHSMR-SG16 (raw) and U-SW10 (decr) combined with $Q > 3$, as this model would boost the clustering signal at all AGN luminosities due to a significant increase in the relative fraction of satellites, hosted in more massive/clustered parent halos, that are active (fourth panel). However, this same model would also predict a $P_{\rm AGN}$ distribution an order of magnitude higher than the observationally derived specific accretion rate distributions (see Figure 6), while models based on the BHSMR–Sha16 (debiased) relation and the U-SW10 (decr) duty cycle would be consistent with it (see Figure 5).

5. Additional Dependencies in the Input Model Parameters

All of the reference models discussed so far to create AGN mock catalogs assume that the input parameters are uncorrelated. In this section, we explore the impact of relaxing this assumption in some of the key parameters in our modeling. As a first case, we assume that the BH, stellar, and halo mass share some degree of correlation. More specifically, we assume that there exists a covariant scatter in the input stellar mass–halo mass relation and the BH mass–stellar mass relation. In practice, we assign to each halo mass a value of $M_{\rm star}$ and $M_{\rm BH}$ from a multivariate Gaussian distribution following the methodology described in Viitanen et al. (2021). A positive covariance would imply that it would be more likely for $M_{\rm BH}$ to be scattered in the same direction as $M_{\rm star}$.

We find that the covariance scatter does not affect the AGN large-scale bias as a function of BH mass and X-ray luminosity. On the contrary, as shown in Figure 7 (lower panels), the AGN bias dependence on host galaxy stellar mass is smoothed out when assuming a covariant scatter, independent of the particular choice of input stellar mass–halo mass and BH mass–stellar mass relation or AGN duty cycle. This behavior is expected, as the end effect of a covariant scatter is to generate a larger scatter in the scaling relations, thus naturally reducing the clustering strength, especially at larger stellar masses. In particular, the covariant scatter model predicts an AGN bias versus $M_{\rm star}$ almost constant, and at $M_{\rm star} \sim 10^{11.5}\ M_\odot$ two times smaller than what predicted by the case without covariance. A model with covariant scatter, i.e., with a

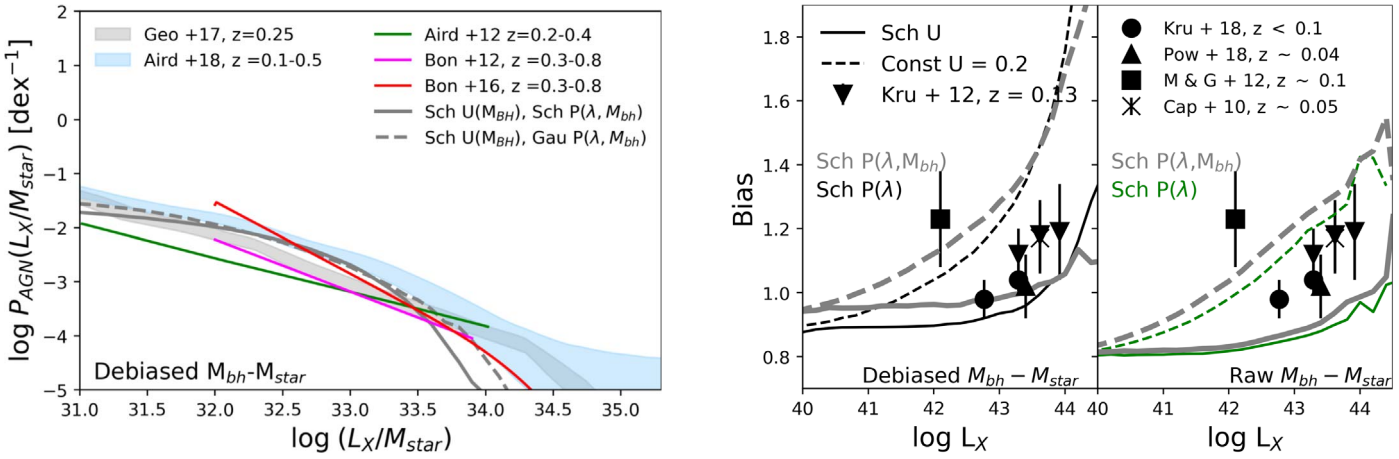

Figure 9. Left panel: specific accretion rate distribution $P_{\rm AGN}(\lambda, M_{\rm star})$ given by the convolution of the input BH mass–dependent Eddington ratio distribution $P(\lambda, M_{\rm BH})$ and AGN duty cycle. The prediction from mock AGNs with a Schechter (solid line) and Gaussian (dashed line) $P(\lambda, M_{\rm BH})$ and an $M_{\rm star}$–$M_{\rm BH}$ relation as defined in Shankar et al. (2016) are compared with data as in Figure 4. Right panel: large-scale bias vs. X-ray (2–10 keV) luminosity (in units of erg s^{-1}) for mock AGNs when using an input Eddington ratio distribution that is independent of (dependent) the BH mass for a decreasing (Schulze & Wisotzki 2010) and constant ($U = 0.2$; Goulding et al. 2010) duty cycle as a function of BH mass, compared with bias estimates from previous studies at similar redshifts.

(positive) correlation between BH mass and galaxy mass at fixed halo mass, would then imply a substantially different bias as a function of the stellar mass at large stellar masses, $M_{\rm star} > 10^{11}\ M_{\odot}$, between AGNs and the overall population of galaxies. In other words, a covariant scatter would inherently imply that AGN host galaxies are not a random selection of galaxies of the same stellar mass. The present data do not allow us to clearly distinguish between models with and without a covariant scatter. In fact, as shown in Figure 7 (lower first panel), currently available AGN bias estimates as a function of stellar mass of SDSS AGNs (Zhang et al. 2021) only extend up to $M_{\rm star} \sim 10^{11.3}\ M_{\odot}$, where the models have just started to diverge (solid gray versus dotted–dashed green lines), although the data tend to be closer to the model without covariant scatter. An AGN clustering measurement at higher host galaxy stellar mass bins will become available in the near future (e.g., Euclid), allowing us to rule out or confirm a covariant scatter at a high confidence level. We stress that, as anticipated above, the model without covariance is in good agreement, as expected, with the bias of SDSS galaxies at $z < 0.1$ (red squares in Figure 7, lower first panel). We will more comprehensively discuss the consequences of a covariant scatter in Viitanen et al. (2021).

As a second relevant case, we explore the effect of using an input Eddington ratio distribution $P(\lambda)$ that also depends on the BH/stellar mass, i.e., $P(\lambda, M_{\rm BH})$. A mass dependence on the input Eddington ratio distribution is expected from, e.g., continuity equation arguments (e.g., Shankar et al. 2013; Aversa et al. 2015), as well as from direct observational measurements (e.g., Kauffmann & Heckman 2009; Georgakakis et al. 2017; Aird et al. 2018). Broadly following the continuity equation model by Aversa et al. (2015; see their Figure 6), we divide our BH mock sample into two groups above and below a dividing mass of $\log M_{\rm BH}\ [M_{\odot}] = 7$ and then assign to each group of BHs Eddington ratios extracted from a Schechter $P(\lambda)$ with the same power-law slope α and a higher characteristic $\langle\lambda\rangle$ for BHs in the lowest mass bin.

As discussed above, we expect that varying the input Eddington ratio distribution will mainly affect two observables, namely the specific accretion rate distribution $P_{\rm AGN}$ and the AGN large-scale bias as a function of X-ray luminosity. Indeed, we verified that all of our main predictions remain unaltered when adopting a mass-dependent $P(\lambda, M_{\rm BH})$ and found only a moderate variation in $P_{\rm AGN}$ (left panel of Figure 9), with a more pronounced tail at higher $L_{\rm X}/M_{\rm star}$, in somewhat better agreement with the data. Similarly, we find that an input $P(\lambda, M_{\rm BH})$ only slightly increases the AGN bias versus $L_{\rm X}$ by $\sim$5%, compared to an input Eddington ratio distribution independent of BH mass (right panel of Figure 9).

All in all, from the tests discussed above, we can conclude that introducing reasonable correlations among the main parameters at play in our model does not significantly alter any of our main results.

6. How to Build Realistic AGN Mocks

In the previous sections, we showed that a large variety of models characterized by distinct $M_{\rm BH}$–$M_{\rm star}$ relations and specific accretion rate distributions $P_{\rm AGN}$ (obtained as a convolution of the input $P(\lambda)$ with the AGN duty cycle U) can create AGN mocks matching the observed AGN XLF. In addition, the corresponding large-scale bias at a given stellar mass is independent of $P_{\rm AGN}$ and the stellar mass–BH mass relation, simply because the bias mostly depends on the parameter Q and the input $M_{\rm star}$–M_h relation. Thus, having characterized a given $P_{\rm AGN}$ that, by design, observationally fits the AGN XLF does not guarantee a unique and valid model to create AGN mocks, even when we consider the clustering at fixed stellar mass, simply because the latter is not affected by the $P_{\rm AGN}$ distribution and the stellar mass–BH mass relation.

The results summarized above imply strong degeneracies among the input parameters used to create mock catalogs of AGNs. Only by considering all of the observables, in particular the AGN large-scale bias as a function of both BH mass and X-ray luminosity, can we break such degeneracies in the input model parameters. Figure 10 provides a summary of the different dependencies of the observables considered in this work on one or more of the model input parameters. Both the AGN XLF and $P_{\rm AGN}$ are highly degenerate, being dependent on several input parameters. On the other hand, the AGN bias as a function of stellar mass only depends on the stellar mass–halo mass relation, once Q is fixed, once Q has been fixed, and in turn also the AGN bias at fixed BH mass depends only on

	Input Parameter				
Observable	P(λ)	U	M_{star} - M_h	M_{bh} - M_{star}	Q
AGN XLF	✓	✓	✓	✓	
P_{AGN}	✓	✓	✓	✓	
b_{gal} - M_{star}			✓		
b_{AGN} - M_{star}			✓		✓
b_{AGN} - M_{bh}			✓	✓	✓
b_{AGN} - L_X	✓	✓		✓	✓
f_{AGNsat}					✓

Figure 10. Dependence of the observables on the input model parameters.

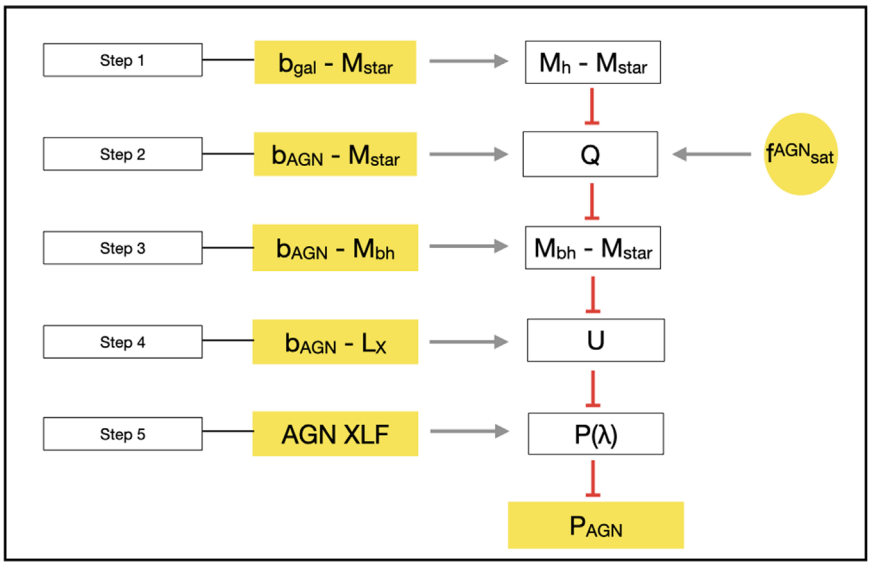

Figure 11. Sketch of how to build realistic AGN mocks. Filled yellow boxes refer to the observables considered in this work. The dependence of each observable on one or a few input model parameters (open black boxes) is shown as red lines. From the comparison of observationally derived relations and the AGN mock catalog predictions, we can constrain (gray arrows) the input parameters. Additional observables, such as the fraction of satellite AGNs (filled yellow circle), can help in breaking the degeneracies among the input model parameters.

the M_{BH}–M_{star} relation, once both Q and the M_{star}–M_h relation have been fixed.

Based on the information contained in Figure 10, in what follows, we provide the different steps to create a robust and realistic mock catalog of AGNs. As sketched in Figure 11, the stellar mass–halo mass relation and the Q parameter can be constrained by combining the large-scale clustering as a function of stellar mass for both galaxies and AGNs (Figure 7, lower panel), at least in the limit in which AGN hosts are a random subsample of all galaxies of similar stellar mass. In particular, our results suggest a model with an input M_{star}–M_h relation as described in Grylls et al. (2019), and $Q \leqslant 2$ is broadly consistent with available data at $z \leqslant 0.1$.

After having fixed the input stellar mass–halo mass relation and Q, the AGN large-scale bias as a function of BH mass can be used to derive the input M_{BH}–M_{star} relation. As already shown in Shankar et al. (2020), we found that a model with a BHSMR–Sha16 (debiased) with $Q \leqslant 2$ better matches the bias estimates as a function of BH mass (Figure 7, upper panel).

Observational constraints on the AGN duty cycle can then be derived from the comparison of the model predictions with the measured AGN large-scale bias as a function of AGN luminosity (Figure 8). A model with BHSMR–Sha16 (debiased), $Q \leqslant 2$, and U-SW10 (decr) is able to reproduce the AGN bias as a function of L_X for both a Gaussian and a Schechter $P(\lambda)$.

Finally, after having fixed the stellar mass–halo mass relation (Grylls et al. 2019), BHSMR–Sha16 (debiased), $Q \leqslant 2$, U-SW10 (decr), the combination of the AGN XLF and the specific accretion rate distribution P_{AGN} allow us to derive the free parameters of the input Eddington ratio distribution, independently of the exact shape of the input $P(\lambda)$.

Estimates of the fraction of active satellites in groups and clusters at the redshift of interest (e.g., Allevato et al. 2012; Leauthaud et al. 2015) can further help to independently constrain the Q parameter (e.g., Gatti et al. 2016). Additional observables can be considered, such as the average L_X–SFR/M_{star} relation, which mostly depends on $P(\lambda)$ and the M_{star}–M_{BH} relation (Carraro et al. 2021).

Our current work thus reveals the right observables that we should focus on to break the degeneracies in the model input parameters and provides the steps to build a robust and realistic AGN mock consistent with many different observables. At the same time, our framework represents an invaluable tool to shed light on the cosmological evolution of BHs, providing key constraints on the underlying scaling relations between BHs, their galaxies, and host dark matter halos, along with information on their accretion rates, frequency (the duty cycle), and environmental dependence (via the Q parameter).

7. Discussion

7.1. Specific Accretion Rate Distribution

In this work, we showed how observables depend on the input model parameters (Figure 10) and how to build step-by-step robust mock catalogs of AGNs that minimize the danger of inner degeneracies and include knowledge of the underlying BH mass and Eddington ratio distributions (Figure 11).

The first observable we considered is the specific accretion rate distribution P_{AGN}, defined as the convolution of the input AGN duty cycle U and normalized Eddington ratio distribution $P(\lambda)$. The P_{AGN} distribution has been intensively studied in the last decade, mostly in X-ray-selected AGN samples (e.g., Bongiorno et al. 2016; Aird et al. 2017, 2018; Georgakakis et al. 2017), and it has been extensively used as the main key observable to generate data-driven AGN mock catalogs (e.g., Comparat et al. 2019; Aird & Coil 2021).

However, when using models uniquely tuned to the measured P_{AGN}, we miss information on individual input parameters, such as the AGN duty cycle U, the Eddington ratio distribution, and the BH mass–stellar mass relation. We in fact showed in the previous sections that, for a fixed M_{BH}–M_{star} relation, widely different combinations of U and $P(\lambda)$ can provide very similar specific accretion rate distributions and AGN XLFs consistent with the data. Moreover, any specific accretion rate distribution P_{AGN} that reproduces the AGN XLF does not affect the AGN large-scale bias at a given stellar mass. Thus, the P_{AGN} distribution and AGN XLF are not suited to constrain the input model parameters when used in isolation.

On the contrary, in this work, we explicitly consider the AGN duty cycle, $P(\lambda)$, and BH mass–stellar mass relation as distinct input model parameters, which we tested against several independent observables, including the large-scale bias as a function of stellar/BH mass and X-ray luminosity. In particular, we found that the comparison of observationally derived P_{AGN} with the predictions of AGN mock catalogs is in better agreement with models that assume an input BH mass–stellar mass relation lower in normalization (which we referred to BHSMR–Sha16, debiased) with respect to what is usually inferred in the local universe from early-type galaxies with dynamically measured BHs (which we referred to as BHSMR-SG16, raw). Our mock also prefers the AGN duty cycle decreasing with BH mass (U-SW10), consistent with what was also derived from continuity equation arguments (e.g., Shankar et al. 2013). The agreement with the data, and in particular with the measured P_{AGN} function, further improves when the input Eddington ratio distribution depends on the BH mass $P(\lambda, M_{BH})$ for both a Gaussian and a Schechter function or, for example, assuming a double power-law distribution (Yang et al. 2019). It is worth noticing that, when considered in isolation, the P_{AGN} distribution can also be reproduced, at least at lower luminosities/stellar masses $\log\lambda \leqslant 33$, by using in input BHSMR-SG16 (raw) and U-M19 (incr) or U-G10 (const) (for both a Gaussian and a Schechter $P(\lambda)$). This degeneracy can be broken by testing the model against additional independent observables, most notably the AGN large-scale clustering.

7.2. Bias versus M_{star}/M_{BH}

The second key observable to consider is indeed the AGN large-scale bias as a function of both stellar mass and BH mass, which is not affected by the input AGN duty cycle and $P(\lambda)$. The large-scale bias as a function of the host galaxy stellar mass is set by the stellar mass–halo mass relation and independent of the AGN model (i.e., the AGN duty cycle, BH mass–stellar mass relation, and Eddington ratio distribution) as long as, as discussed above, the AGN host galaxies are a random subsample of the galaxies with similar stellar mass. Georgakakis et al. (2019) also found that the level of clustering of AGN samples primarily correlates with the stellar masses of their host galaxies, rather than their instantaneous accretion luminosities.

As shown in Shankar et al. (2020), the AGN large-scale bias as a function of BH mass can instead effectively be used to put constraints on the BH mass–stellar mass relation and the parameter Q, the ratio of satellite and central active galaxies/BHs. In detail, Shankar et al. (2020) found that the observed bias of AGNs at $z = 0.25$ (Krumpe et al. 2015) can be reproduced by assuming BHSMR–Sha16 (debiased) and $Q \leqslant 2$, which corresponds to satellite AGN fractions $f_{sat}^{AGN} \leqslant 0.15$. A similar value ($f_{sat}^{AGN} \sim 0.18$) has been suggested by Leauthaud et al. (2015) for COSMOS AGNs at $z < 1$. Allevato et al. (2012) performed direct measurement of the halo occupation distribution (HOD) for COSMOS AGNs based on the mass function of galaxy groups hosting AGNs and found that the duty cycle of satellite AGNs is comparable to or slightly larger than that of central AGNs, i.e., $Q \leqslant 2$. A very low value of the Q parameter would be in line with quasars hosted in central galaxies that more frequently undergo mergers with other galaxies (Hopkins et al. 2008). On the other hand, a relatively high value of Q would suggest that triggering mechanisms other than mergers, such as secular processes and bar instabilities, are equally or even more efficient in producing luminous AGNs (e.g., Georgakakis et al. 2009; Allevato et al. 2011; Gatti et al. 2016). The SEM model used in Georgakakis et al. (2019) for populating halos with AGNs does not distinguish between central and satellite active BHs; i.e., effectively, their model adopts $Q = 1$, which implies a satellite fraction of $f_{sat}^{AGN} \sim 10\%$–20%. Georgakakis et al. (2019) claimed, as also found here, that the fair agreement of their mocks with the observationally derived AGN HOD (e.g., Allevato et al. 2012; Miyaji et al. 2011; Shen et al. 2013) supports low values of the Q parameter.

We find that a model with an input BHSMR–Sha16 (debiased) and $Q \leqslant 2$ does indeed better match the large-scale bias as a function of BH mass of X-ray AGNs at $z < 0.1$ (Powell et al. 2018), further extending the results of Shankar

et al. (2020) at even lower redshifts. Additionally, the same model is in better agreement with observationally inferred $P_{\rm AGN}$ distributions. This model also assumes (i) a stellar mass–halo mass relation as derived in Grylls et al. (2019), which reproduces the most recent estimates of the local galaxy stellar mass function by Bernardi et al. (2017), and it is consistent, as shown in Figure 7, with the large-scale clustering of local central AGNs in SDSS (Zhang et al. 2021) and SDSS galaxies with photometry from Domínguez Sánchez et al. (2018); and (ii) a parameter $Q \leqslant 2$ as suggested by observations of the AGN satellite fraction at low redshifts (e.g., Allevato et al. 2012; Leauthaud et al. 2015).

A model with BHSMR-SG16 (raw) with U-M19 (incr) or U-G10 (const) would instead require high values of the Q parameter ($Q > 3$) and/or an input stellar mass–halo mass relation as derived by Moster et al. (2013). More importantly, the latter model is inconsistent with the large-scale bias versus X-ray luminosity inferred for X-ray AGNs at similar redshift (e.g., Krumpe et al. 2018; Powell et al. 2018), independent of the choice of the input $P(\lambda)$ distribution.

It is worth noticing that our results in terms of AGN large-scale bias as a function of stellar/BH mass are not affected by the choice of a BH mass–dependent input $P(\lambda, M_{\rm BH})$. On the contrary, the covariant scatter smooths out the large-scale bias dependence on the stellar mass for mock AGNs, especially at $M_{\rm star} > 10^{11}\ M_{\odot}$. Currently available bias estimates of SDSS AGNs (Zhang et al. 2021) favor models for the creation of mock catalogs without covariant scatter, at least at $z \sim 0.1$. In the near future, clustering measurements of AGNs that extend up to $M_{\rm star} > 10^{11}\ M_{\odot}$ will allow us to confirm these results (see Viitanen et al. 2021, for a more comprehensive discussion of the role of covariant scatter at $z \sim 1$).

7.3. *Bias versus* L_X

The large-scale AGN bias as a function of X-ray luminosity represents an additional crucial and powerful diagnostic to constrain viable AGN models, as it is strongly dependent on the input AGN duty cycle but weakly dependent on the input stellar mass–halo mass relation or $P(\lambda)$ distribution (Figure 8). The large-scale bias as a function of luminosity for mock AGNs has been investigated in Georgakakis et al. (2019) and Aird & Coil (2021) at different redshifts. Their SEMs predict a negligible or extremely weak dependence of the AGN clustering on accretion luminosity. We also found an almost constant relation between the bias and the AGN X-ray luminosity, especially when using U-SW10 (decr), independent of the particular choice of the stellar mass–halo mass relation, BH mass–stellar mass relation, and $P(\lambda)$.

Measurements of the bias dependence on L_X for X-ray-selected AGNs at $z \leqslant 0.1$ (e.g., Krumpe et al. 2018; Powell et al. 2018) can be reproduced in the models presented in this work assuming (i) U-SW10 (decr) and BHSMR–Sha16 (debiased) with $Q \leqslant 2$ or (ii) BHSMR-SG16 (raw) with $Q > 3$. This is valid for both a Schechter and a Gaussian $P(\lambda)$ or $P(\lambda, M_{\rm BH})$. However, in the latter case, the corresponding specific accretion rate distribution $P_{\rm AGN}$ would be almost an order of magnitude higher than observations. Georgakakis et al. (2019) and Aird & Coil (2021) also compared AGN bias estimates and/or halo mass as a function of luminosity with mock AGN predictions. At redshift $z \sim 0.25$–0.3, they found a small offset with respect to measurements that requires revisiting some of their model input assumptions and could be due to selection effects of specific samples, e.g., redshift interval and X-ray flux limits.

As discussed in the previous section, only the combination of all of the observables, namely the AGN XLF, the $P_{\rm AGN}$ distribution, the AGN large-scale bias as a function of stellar/BH mass, and L_X, can break the degeneracy in the input model parameters and ensure the creation of realistic AGN mock catalogs.

8. Conclusions

In this work, we describe a step-by-step methodology to create robust, transparent, and physically motivated AGN mock catalogs that can be safely used for extragalactic large-scale surveys and as a test bed for cosmological models of BH and galaxy coevolution. Our methodology, summarized in Figure 11, allows us to minimize the danger of degeneracies and pin down the underlying physical properties of BHs in terms of their accretion distributions and links to their host galaxies. More specifically, we find the following.

1. The AGN XLF and specific accretion rate distribution $P_{\rm AGN}$ depend on the input $M_{\rm BH}$–$M_{\rm star}$ and $M_{\rm star}$–M_h relations, Eddington ratio distribution $P(\lambda)$, and AGN duty cycle U and are independent of the particular choice of Q, parameterizing the ratio between satellite and central AGNs at a given host galaxy stellar mass.
2. The clustering at fixed stellar mass only depends on the $M_{\rm star}$–M_h relation and the Q parameter.
3. The clustering at fixed BH mass only depends on the $M_{\rm BH}$–$M_{\rm star}$ and $M_{\rm star}$–M_h relations and the Q parameter.
4. All AGN mocks built on empirically based $M_{\rm star}$–M_h relations will broadly match the AGN clustering at a given stellar mass, provided the AGN hosts are a random subsample of the underlying galaxy population of the same stellar mass.
5. A large variety of specific accretion rate distributions $P_{\rm AGN}$, defined as the convolution of the normalized Eddington ratio distribution $P(\lambda)$ and the AGN duty cycle U, can reproduce the AGN XLF, even if characterized by widely different underlying $M_{\rm BH}$–$M_{\rm star}$ and/or duty cycles and/or $P(\lambda)$.
6. Only the combination with additional observables, most notably the AGN large-scale bias as a function of BH mass and X-ray luminosity, can break the (strong) degeneracies in the input model parameters.

The results listed above indeed imply strong degeneracies among the input parameters used to create mock catalogs of AGNs. Having characterized a given $P_{\rm AGN}$ that, by design, observationally fits the AGN XLF does not guarantee a unique and valid solution to create realistic AGN mocks, even when we consider the clustering at fixed stellar mass, simply because the latter is mostly dependent on Q and the $M_{\rm star}$–M_h relation.

The AGN large-scale bias as a function of both BH mass and X-ray luminosity is a crucial diagnostic for all AGN models. In particular, a model with an input stellar mass–halo mass relation calibrated from detailed abundance matching (e.g., Grylls et al. 2019), an $M_{\rm BH}$–$M_{\rm star}$ with lower normalizations than those usually inferred for dynamically measured local BHs (e.g., Reines & Volonteri 2015; Shankar et al. 2016), and an AGN duty cycle decreasing with BH mass (e.g., Schulze & Wisotzki 2010), combined with the assumption that central and satellite BHs of equal mass share similar probabilities of being

active (i.e., $Q \leqslant 2$), generates a mock catalog of AGNs that matches the observationally constrained AGN XLF, $P_{\rm AGN}$, and AGN large-scale bias as a function of the stellar/BH mass and X-ray luminosity at $z \leqslant 0.1$. We stress that the methodology outlined in this work is of wide applicability, and we expect it to hold at all redshifts, thus allowing us to constrain the evolution in the BH scaling relations, duty cycles, and Eddington ratio distributions (e.g., Viitanen et al. 2021).

Additional observables, not included in the present work, can also be considered to set stronger/additional constraints on the input model parameters, for instance, the average $L_{\rm X}$–SFR/$M_{\rm star}$ relation, which mostly depends on the input Eddington ratio distribution $P(\lambda)$ and the $M_{\rm BH}$–$M_{\rm star}$ relation (Carraro et al. 2021). Estimates of the fraction of active satellites in groups and clusters at low redshift (e.g., Allevato et al. 2012; Leauthaud et al. 2015) are also key observables to independently constrain the Q parameter (e.g., Gatti et al. 2016).

Our present study provides a complete framework to build robust and realistic AGN theoretical samples consistent with diverse and largely independent observables, and it is capable of setting strong constraints on the main parameters controlling the growth of BHs in galaxies. Our work can thus provide key insights into cosmological galaxy evolution models while defining a clear strategy to produce robust galaxy mock catalogs for imminent large-scale galaxy surveys such as Euclid and LSST.

We thank the anonymous referee for carefully reading the manuscript and providing us with constructive remarks. V.A. acknowledge support from MUR-SNS-2019. V. A. is grateful to "ROST" and Cinesaibai for the amazing soundtrack (www.youtube.com/watch?v=qDCl-oK9HqI). F.S. acknowledge partial support from a Leverhulme Trust Research Fellowship. F.S. warmly thanks David Weinberg for many useful discussions. A.V. is grateful to the Vilho, Yrjö and Kalle Väisälä Foundation of the FinnishAccademy of Science and Letters. C.M. We acknowledge extensive use of the Python libraries Colossus, Corrfunc, astropy, matplotlib, numpy, pandas, and scipy. The MultiDark Database used in this paper and the web application providing online access to it were constructed as part of the activities of the German Astrophysical Virtual Observatory as the result of a collaboration between the Leibniz-Institute for Astrophysics Potsdam (AIP) and the Spanish MultiDark Consolider Project CSD2009-00064. The Bolshoi and MultiDark simulations were run on NASA's Pleiades supercomputer at the NASA Ames Research Center. The MultiDark-Planck (MDPL) and the BigMD simulation suite have been performed on the Supermuc supercomputer at LRZ using time granted by PRACE.

Data Availability

The MultiDark ROCKSTAR halo catalogs are available in the CosmoSim database at https://www.cosmosim.org/. Other data underlying this article will be shared on reasonable request to the corresponding author.

ORCID iDs

V. Allevato https://orcid.org/0000-0001-7232-5152
F. Shankar https://orcid.org/0000-0001-8973-5051
C. Marsden https://orcid.org/0000-0002-7993-6228
A. Viitanen https://orcid.org/0000-0001-9383-786X
A. Georgakakis https://orcid.org/0000-0002-3514-2442
A. Ferrara https://orcid.org/0000-0002-9400-7312
A. Finoguenov https://orcid.org/0000-0002-4606-5403

References

Aird, J., & Coil, A. L. 2021, MNRAS, 502, 5962
Aird, J., Coil, A. L., & Georgakakis, A. 2017, MNRAS, 465, 3390
Aird, J., Coil, A. L., & Georgakakis, A. 2018, MNRAS, 474, 1225
Aird, J., Coil, A. L., & Georgakakis, A. 2019, MNRAS, 484, 4360
Aird, J., Coil, A. L., Moustakas, J., et al. 2012, ApJ, 746, 90
Allevato, V., Finoguenov, A., Cappelluti, N., et al. 2011, ApJ, 736, 99
Allevato, V., Finoguenov, A., Hasinger, G., et al. 2012, ApJ, 758, 47
Allevato, V., Viitanen, A., Finoguenov, A., et al. 2019, A&A, 632, A88
Aversa, R., Lapi, A., de Zotti, G., Shankar, F., & Danese, L. 2015, ApJ, 810, 74
Baldry, I. K., Driver, S. P., Loveday, J., et al. 2012, MNRAS, 421, 621
Behroozi, P. S., Wechsler, R. H., & Conroy, C. 2013a, ApJ, 770, 57
Behroozi, P. S., Wechsler, R. H., & Wu, H.-Y. 2013b, ApJ, 762, 109
Bell, E. F., McIntosh, D. H., Katz, N., & Weinberg, M. D. 2003, ApJS, 149, 289
Bernardi, M., Meert, A., Sheth, R. K., et al. 2017, MNRAS, 467, 2217
Bernardi, M., Shankar, F., Hyde, J. B., et al. 2010, MNRAS, 404, 2087
Bongiorno, A., Merloni, A., Brusa, M., et al. 2012, MNRAS, 427, 3103
Bongiorno, A., Schulze, A., Merloni, A., et al. 2016, A&A, 588, A78
Carraro, R., Shankar, F., Allevato, V., et al. 2021, ApJL, submitted
Comparat, J., Merloni, A., Salvato, M., et al. 2019, MNRAS, 487, 2005
Conroy, C., & White, M. 2013, ApJ, 762, 70
Davis, B. L., Graham, A. W., & Cameron, E. 2018, ApJ, 869, 113
Domínguez Sánchez, H., Huertas-Company, M., Bernardi, M., Tuccillo, D., & Fischer, J. L. 2018, MNRAS, 476, 3661
Duras, F., Bongiorno, A., Ricci, F., et al. 2020, A&A, 636, A73
Eisenstein, D. J., & Hu, W. 1999, ApJ, 511, 5
Gatti, M., Shankar, F., Bouillot, V., et al. 2016, MNRAS, 456, 1073
Georgakakis, A., Aird, J., Schulze, A., et al. 2017, MNRAS, 471, 1976
Georgakakis, A., Coil, A. L., Laird, E. S., et al. 2009, MNRAS, 397, 623
Georgakakis, A., Comparat, J., Merloni, A., et al. 2019, MNRAS, 487, 275
González, J. E., Lacey, C. G., Baugh, C. M., & Frenk, C. S. 2011, MNRAS, 413, 749
Goulding, A. D., Alexander, D. M., Lehmer, B. D., & Mullaney, J. R. 2010, MNRAS, 406, 597
Grylls, P. J., Shankar, F., & Conselice, C. J. 2020a, MNRAS, 499, 2265
Grylls, P. J., Shankar, F., Leja, J., et al. 2020b, MNRAS, 491, 634
Grylls, P. J., Shankar, F., Zanisi, L., & Bernardi, M. 2019, MNRAS, 483, 2506
Heckman, T. M., & Kauffmann, G. 2006, NewAR, 50, 677
Hickox, R. C., Jones, C., Forman, W. R., et al. 2009, ApJ, 696, 891
Hopkins, P. F., & Hernquist, L. 2009, ApJ, 698, 1550
Hopkins, P. F., Hernquist, L., Cox, T. J., et al. 2006, ApJS, 163, 1
Hopkins, P. F., Hernquist, L., Cox, T. J., & Kereš, D. 2008, ApJS, 175, 356
Kauffmann, G., & Heckman, T. M. 2009, MNRAS, 397, 135
Klypin, A., Yepes, G., Gottlöber, S., Prada, F., & Heß, S. 2016, MNRAS, 457, 4340
Kormendy, J., & Ho, L. C. 2013, ARA&A, 51, 511
Kravtsov, A. V., Berlind, A. A., Wechsler, R. H., et al. 2004, ApJ, 609, 35
Kravtsov, A. V., Vikhlinin, A. A., & Meshcheryakov, A. V. 2018, AstL, 44, 8
Krumpe, M., Miyaji, T., Coil, A. L., & Aceves, H. 2018, MNRAS, 474, 1773
Krumpe, M., Miyaji, T., Husemann, B., et al. 2015, ApJ, 815, 21
Lapi, A., Salucci, P., & Danese, L. 2018, ApJ, 859, 2
Laureijs, R., Amiaux, J., Arduini, S., et al. 2011, arXiv:1110.3193
Leauthaud, A. J., Benson, A., Civano, F., et al. 2015, MNRAS, 446, 1874
LSST Science Collaboration, Abell, P. A., Allison, J., et al. 2009, arXiv:0912.0201
Man, Z.-Y., Peng, Y.-J., Kong, X., et al. 2019, MNRAS, 488, 89
Marconi, A., Risaliti, G., Gilli, R., et al. 2004, MNRAS, 351, 169
Meert, A., Vikram, V., & Bernardi, M. 2015, MNRAS, 446, 3943
Meert, A., Vikram, V., & Bernardi, M. 2016, MNRAS, 455, 2440
Menci, N., Fiore, F., Puccetti, S., & Cavaliere, A. 2008, ApJ, 686, 219
Miyaji, T., Hasinger, G., Salvato, M., et al. 2015, ApJ, 804, 104
Monaco, P., Fontanot, F., & Taffoni, G. 2007, MNRAS, 375, 1189
Moster, B. P., Naab, T., & White, S. D. M. 2013, MNRAS, 428, 3121
Moustakas, J., Coil, A. L., Aird, J., et al. 2013, ApJ, 767, 50
Nuñez-Castiñeyra, A., Nezri, E., Devriendt, J., & Teyssier, R. 2020, MNRAS, 501, 62

O'Leary, J. A., Moster, B. P., & Krämer, E. 2021, MNRAS, 503, 5646
Powell, M. C., Cappelluti, N., Urry, C. M., et al. 2018, ApJ, 858, 110
Reines, A. E., & Volonteri, M. 2015, ApJ, 813, 82
Riebe, K., Partl, A. M., Enke, H., et al. 2013, AN, 334, 691
Sahu, N., Graham, A. W., & Davis, B. L. 2019, ApJ, 876, 155
Savorgnan, G. A. D., & Graham, A. W. 2016, ApJS, 222, 10
Scannapieco, C., Wadepuhl, M., Parry, O. H., et al. 2012, MNRAS, 423, 1726
Schulze, A., & Wisotzki, L. 2010, A&A, 516, A87
Shankar, F., Allevato, V., Bernardi, M., et al. 2020, NatAs, 4, 282
Shankar, F., Bernardi, M., Richardson, K., et al. 2019, MNRAS, 485, 1278
Shankar, F., Bernardi, M., Sheth, R. K., et al. 2016, MNRAS, 460, 3119
Shankar, F., Lapi, A., Salucci, P., De Zotti, G., & Danese, L. 2006, ApJ, 643, 14
Shankar, F., Mei, S., Huertas-Company, M., et al. 2014, MNRAS, 439, 3189
Shankar, F., Sonnenfeld, A., Mamon, G. A., et al. 2017, ApJ, 840, 34
Shankar, F., Weinberg, D. H., & Miralda-Escudé, J. 2009, ApJ, 690, 20
Shankar, F., Weinberg, D. H., & Miralda-Escudé, J. 2013, MNRAS, 428, 421
Small, T. A., & Blandford, R. D. 1992, MNRAS, 259, 725
Springel, V., White, S. D. M., Jenkins, A., et al. 2005, Natur, 435, 629
Steed, A., & Weinberg, D. H. 2003, arXiv:astro-ph/0311312
Tinker, J. L., Weinberg, D. H., Zheng, Z., & Zehavi, I. 2005, ApJ, 631, 41
Ueda, Y., Akiyama, M., Hasinger, G., Miyaji, T., & Watson, M. G. 2014, ApJ, 786, 104
Vale, A., & Ostriker, J. P. 2004, MNRAS, 353, 189
van den Bosch, F. C. 2002, MNRAS, 331, 98
Viitanen, A, Allevato, V., Finoguenov, A., et al. 2021, MNRAS, submitted
Yang, G., Brandt, W. N., Alexander, D. M., et al. 2019, MNRAS, 485, 3721
Zhang, Z., Wang, H., Luo, W., et al. 2021, A&A, 650, A155